of protons needed to detach two $Al(H_2O)_6^{3+}$ species is: $24 - 3w - 3x - 3y - 3z$, where w, x, y and z are the number of protons at equilibrium on four-, three-, two- and single-coordinated oxygens. There are three of each oxygen type [*4*, *3*, *2*, *1*] in the reaction, and not two as in the case of goethite (Table 1). The newly exposed bulk sites consume $3w$ protons to achieve equilibrium at the surface and the nine vacated coordination sites react with water molecules and release $(18 - 3x - 3y - 3z)$ protons to achieve their equilibrium protonation states. The net number of protons consumed by steady-state reaction is: $6 = (24 - 3w - 3x - 3y - 3z) - (18 - 3x - 3y - 3z) + 3w$ or three protons per aluminium; $n = 3$, as observed in some[8,17] but not all[13] experiments.

Each monoatomic step on these minerals is essentially a polymer of identical linked metal-oxide polyhedra. The $M(H_2O)_6^{z+}$ monomer detaching from these steps has 12 protons, but the net number of protons transferred from the aqueous solution to each metal before detachment is much smaller than 12. In these examples, it equals the metal valence and the proton rate order, and reflects the stoichiometry on the detaching complex. If, for example, $Fe(H_2O)_5(OH)^{2+}$ detaches from the geothite surface in acid solutions, $n = 2$ not $n = 3$. Other cases where n does not equal the metal valence probably indicate that the experimental surfaces are not at a steady state[27]; data from experiments on mixed-oxide minerals are complicated by cation leaching and should not be fully trusted[27,28].

Although here we focus on proton reactions, this dissolution mechanism is general and requires a fundamental reassessment of the existing rate laws and reaction models. By assigning ligand functional groups to metal-coordination sites, one can easily demonstrate that ligand-promoted dissolution is rarely independent of adsorbed protons. In addition, rates of reductive dissolution can be organized into classes where either electron transfer or metal detachment is slow. For the latter class, rate orders and reactivities can be predicted in the same way as here, because movement of water molecules from the bulk solution to the inner-coordination sphere of a metal controls the reaction rates. □

Received 12 February; accepted 24 April 1996.

1. Blesa, M. A., Morando, P. J. & Regazzoni, A. E. *Chemical Dissolution of Metal Oxides* (CRC, Boca Raton, FL, 1994).
2. Kuhn, D. C. & Demers, L. M. J. *Toxicology and Environmental Health* **35,** 39–50 (1992).
3. Hochella, M. F. in *Health Effects of Mineral Dusts* (eds Guthrie, D. G. & Mossman, B. T.) 275–305 (Rev. Mineral. **28**, Mineral. Soc. Am., 1993).
4. Hilgard, E. W. *Soils: Their Formation, Properties, Compositions and Relations to Climate and Plant Growth in the Humid and Arid Regions* 19 (MacMillan, New York, 1914).
5. Davis, J. A. & Leckie, J. O. in *Chemical Modeling in Aqueous Systems* (ed. Jenne, E. A.) (Am. chem. Soc., Washington DC, 1979).
6. Wirth, G. S. & Gieskes, J. M. *J. Colloid Interface Sci.* **68,** 492–500 (1979).
7. Blum, A. & Lasaga, A. C. *Geochim. cosmochim. Acta* **55,** 2193–2201 (1991).
8. Furrer, G. & Stumm, W. *Geochim. cosmochim. Acta* **50,** 1847–1860 (1986).
9. Wieland, E., Wehrli, B. & Stumm, W. *Geochim. cosmochim. Acta* **52,** 1969–1981 (1988).
10. Ganor, J., Mogollòn, J. L. & Lasaga, A. C. *Geochim. cosmochim. Acta* **59,** 1037–1053 (1995).
11. Stumm, W. *Chemistry of the Solid–Water Interface* (Wiley, New York, 1992).
12. Stumm, W. & Wollast, R. *Rev. Geophys.* **28,** 53–69 (1990).
13. Carroll-Webb, S. A. & Walther, J. V. *Geochim. cosmochim. Acta* **52,** 2609–2623 (1988).
14. Pulfer, K., Schindler, P. W., Westall, J. C. & Grauer, R. *J. Colloid Interface Sci.* **101,** 554–564 (1984).
15. Oelkers, E. H. & Schott, J. *Geochim. cosmochim. Acta* **59,** 5039–5054 (1995).
16. Guy, C. & Schott, J. *Chem. Geol.* **78,** 181–204 (1989).
17. Ludwig, C. & Casey, W. H. *J. Colloid Interface Sci.* **178,** 176–185 (1996).
18. Furrer, G. thesis, ETH Zurich (1985).
19. Casey, W. H. *J. Colloid Interface Sci.* **146,** 586–589 (1991).
20. Casey, W. H. & Westrich, H. R. *Nature* **355,** 157–159 (1992).
21. Ludwig, C., Casey, W. H. & Rock, P. A. *Nature* **375,** 44–47 (1995).
22. Dove, P. M. & Czank, C. A. *Geochim. cosmochim Acta* **59,** 1907–1916 (1995).
23. Hachiya, K., Sasaki, M., Ikeda, T., Mikami, N. & Yasunaga, T. *J. phys. Chem.* **88,** 27–31 (1984).
24. Ludwig, C., Devidal, J.-L. & Casey, W. H. *Geochim. cosmochim. Acta* **60,** 213–224 (1996).
25. Gratz, A. J., Manne, S. & Hansma, P. K. *Science* **251,** 1343–1346 (1991).
26. Hochella, M. F. in *Mineral–Water Interface Geochemistry* (eds Hochella, M. F. & White, A. F.) Ch. 3 (Rev. Mineral. **23,** Mineral. Soc. Am., Washington DC, 1990).
27. Casey, W. H., Westrich, H. R., Banfield, J. F., Feruzzi, G. & Arnold, G. *Nature* **366,** 253–256 (1993).
28. Casey, W. H. & Bunker, B. in *Mineral–Water Interface Geochemistry* (eds Hochella, M. F. & White, A. F.) Ch. 9 (Rev. Mineral. **23,** Mineral. Soc. Am., Washington DC, 1990).

ACKNOWLEDGEMENTS. We thank Drs. G. Sposito, W. Stumm, P. Rock, B. Phillips, J. Banfield and H. Westrich for helpful discussions and R. Higashi for the photograph of Fig. 3. Support was from the US NSF and DOE.

CORRESPONDENCE should be addressed to W.H.C. (e-mail: whcasey@ucdavis.edu) or C.L. (e-mail: christian.ludwig@eawag.ch).

Emplacement of the Taupo ignimbrite by a dilute turbulent flow

W. Brian Dade & Herbert E. Huppert

Institute of Theoretical Geophysics, Department of Earth Sciences and Department of Applied Mathematics & Theoretical Physics, University of Cambridge, Cambridge CB2 3EQ, UK

An ignimbrite is a pumice-rich deposit that records the passage of a ground-hugging ash flow (a 'pyroclastic flow') generated by the collapse of a volcanic eruption column[1]. Geologists study such deposits to reconstruct the parent eruptions and to predict the consequences of future eruptions. The 1,800-yr-old Taupo ignimbrite of New Zealand has been interpreted to represent *en masse* emplacement by an avalanche-like flow with a volumetric solids concentration in excess of 30% (ref. 2). The evidence for this is equivocal, however, and here we propose the alternative view that the deposit was emplaced by a relatively dilute and turbulent density current[3]. We present an isothermal, hydraulic model, the results of which, taken together with existing observations, suggest that the total flow rate of solids and gas was about 40 $km^3 s^{-1}$ for around 15 minutes. This intense flux resulted in a flow which had a near-vent solids concentration of 0.3% by volume, was about 1 km thick, and travelled outward from the vent with a typical speed of 200 $m s^{-1}$. In view of the good agreement between predicted and observed radial trends in the Taupo deposit, we suggest that the origin of other ignimbrites with similar characteristics should be reconsidered.

The Taupo eruption of 1.8 kyr ago was one of the largest explosive eruptions of the past 10,000 years (ref. 4), and Wilson's detailed account[2] of the Taupo ignimbrite makes it the best-documented deposit of its kind. The ignimbrite comprises about 30 km^3 of material spread over 20,000 km^2 of terrain with low regional slope, and is axisymmetrically distributed around the inferred vent. Owing to its widespread nature, the Taupo deposit is universally regarded as a 'low-aspect-ratio ignimbrite', which resulted from an extremely explosive eruption[5]. The mechanism of emplacement of this and similar deposits, however, is currently one of the most contentious issues in volcanology[6], and features of the Taupo deposit often cited by field geologists as evidence for a densely concentrated parent flow are the subject of continuing debate. For example, intense particle segregation associated with ingestion of ambient air overrun by the flow front, documented by the presence of a relatively coarse, bipartite basal layer ('layer 1'), is not unique to a densely concentrated granular flow. On the contrary, it is only for turbulent, dilute gravity currents that significant entrainment of ambient fluid into the region of the flow front has been well established[7–9]. Similarly, gas-escape and particle-segregation structures in the main body of the deposit, previously taken to reflect the importance of fluidization as a support mechanism in the parent flow, are now recognized as potential products of late-stage depositional processes unrelated to the dynamics of the regional transport system[10,11].

The fact that extremely large, individual pumices with diameters of up to 60 cm were transported to distances of 45 km from the vent has been among the strongest arguments invoked against a turbulent parent flow[2,12]. A dilute, turbulent flow should produce a deposit in which particles are (approximately) aerodynamically equivalent, that is, one in which particles with similar settling velocities are found together in similar proportions. Thus it has been argued that the far-travelled pumice boulders could only have 'floated' to their point of rest on a parent flow in which the density of the matrix of fines exceeded that of individual pumice boulders. This reasoning is based on incorrect notions of settling of particles with individual diameters in excess of about

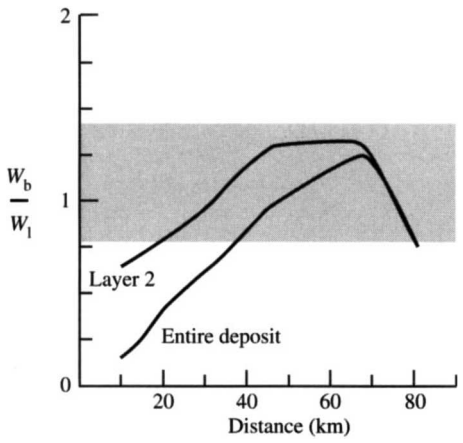

FIG. 1 Ratio of settling velocities of largest pumice boulders (W_b) and lithic fragments (W_l) with nominal densities of 350 kg m^{-3} and 2,500 kg m^{-3}, respectively, as a function of radial distance from the vent. Settling velocities are calculated with the analytical approximation used in our model (see Box 1) for maximal sizes reported by Wilson[2] for layer 2 and for the entire deposit. The shaded region indicates the range of values that correspond to approximate aerodynamic equivalence, which accommodates the observed range of densities of respective particle types. The low values near the vent probably reflect source-controlled scarcity of large pumices overall and the presence of reworked, pre-existing lithics in layer 1.

0.1 mm in low-density gases[13–15]. The settling velocity of such particles is approximately $(g\rho' d)^{1/2}$, where g is the acceleration due to gravity, ρ' is the ratio of particle-to-gas phase densities, and d is nominal diameter of the particle. Given that the density of boulders of large pumice ρ_b is 200–500 kg m^{-3} and that of lithic fragments ρ_l is 2,400–2,700 kg m^{-3} (ref. 2), the ratio of the diameter of the largest pumices to that of the largest lithics should be 5–14 for the largest particles of either type to be in aerodynamic equivalence. Alternatively, the ratio of settling velocities $W_b/W_l \approx [(\rho' d)_b/(\rho' d)_l]^{1/2}$ should be approximately unity at all transport distances. This is the case (Fig. 1). The presence of pumice boulders in the Taupo ignimbrite at large transport distances is entirely consistent with emplacement by a dilute, turbulent flow.

Additional confirmation that the deposit was emplaced by such a flow comes from the degree to which individual grains are sorted by size in the transport direction (Fig. 2*b*, *c*). These patterns are not generally seen in deposits emplaced by debris avalanches[16], a commonly invoked analogue for densely concentrated pyroclastic flows. Distal fining is common, on the other hand, in deposits emplaced by dilute, turbulent gravity currents in other settings[17]. In particular, the combination of massive bedding with little or no vertical grading at a given locality and well defined lateral sorting indicates that rapid deposition took place from a vertically well-mixed suspension of particles in a horizontally non-uniform, turbulent flow subject to constant flux and sediment supply for the limited duration of the event[18].

To evaluate quantitatively the concentration of the Taupo flow, we report here the results of a general hydraulic model for a deposit-forming gravity current[19], modified to accommodate a range of grain sizes in the driving suspension. The model describes the runout of a turbulent gravity current subject to a constant flux at the vent and which spreads over a landscape of small regional slope. It incorporates quantitative expressions for the evolution of flow volume, a Froude-number condition at the flow front, and the gravitational settling of particles from the driving suspension in the body of the flow (see Box 1).

The effects of entrainment of ambient air, time-dependent thermodynamics and compressibility are not considered in describing the deposit-forming flow, and we assume that the driving suspension is sufficiently dilute that interactions between suspended particles are negligible. The model works well even when the density contrast between the ambient fluid and the gravity current is large[20], and in particular for subaqueous deposit-forming currents with solids concentrations of up to 30% by volume[21]. Thus by 'dilute' we mean volumetric solids concentrations less than 30%. We suggest that this approach includes the essential physical processes that govern the runout behaviour of a wide class of deposit-forming gravity currents. In geological terms, the model describes the regional transport system that gives rise to

BOX 1 Equations describing a radially spreading gravity current

We describe the propagation of a deposit-forming current by solving the governing axisymmetric equations for a flow in which the total flux is constant[19]. These have solutions that agree well with numerical treatment of the full equations[28]. The current radius $R(t)$, thickness $h(t)$, speed $U(t)$ and solids concentration $C(t)$ are related to the total flux Q and the settling velocity W by

$$Q = 2\pi RhU, \quad U = dR/dT = \mathrm{Fr}[g'_p(C - C_*)h]^{1/2}, \quad \frac{dC}{dt} = -WC/h \tag{1}$$

where $\mathrm{Fr} \approx 1$ is the Froude number at the head of the current propagating over relatively flat terrain[19], and $g'_p = (\rho_p - \rho_l)g/\rho_a$ is the reduced gravity of the current expressed in terms of g, the acceleration due to gravity, and ρ_p, ρ_l and ρ_a, the densities of individual particles, interstitial gas and ambient air, respectively. The term $C_* = (\rho_a - \rho_l)/(\rho_p - \rho_l)$ represents the concentration of suspended solids at which the flow becomes positively buoyant. The equations given in (1) represent, respectively, conservation of total flux, hydraulic control at the head and the loss of particles through sedimentation.

The settling velocity W of a speroidal particle with nominal diameter d falling through an interstitial gas with kinematic viscosity ν is

$$W = \nu/d[(81 + \eta_*)^{1/2} - 9] \tag{2}$$

where $\eta_* = g'_p\rho_a d^3/\rho_l \nu^2$. Equation (2) is derived from the balance between gravitational and drag forces which govern the settling of individual particles and for which the drag coefficient is $1 + 24\nu/Wd$. It is a useful approximation for all particle sizes.

When modified to accommodate the probability distribution $p(\phi)$ of particle settling speeds in the initial suspension in terms of the logarithmically transformed particle size ϕ, the total solids concentration in the flow at radial distance R is

$$C = C_o \int_{-\infty}^{\infty} \exp[-\pi W(\phi)R^2/Q]p(\phi)d\phi \tag{3}$$

where C_o is constrained to lie between C_* and a value required by conservation of sedimentary mass.

The deposit thickness is given by

$$D = D_o \int_{-\infty}^{\infty} W(\phi)\exp[-\pi W(\phi)R^2/Q]p(\phi)d\phi \Big/ \int_{-\infty}^{\infty} W(\phi)p(\phi)d\phi \tag{4}$$

where D_o is the observed thickness of the deposit near the vent. The composition of the deposit at a distance R comes directly from that of the overlying suspension. Hence the relative amount of material C_d equal to or finer than size ϕ_d that is preserved in the deposit at R is given by

$$C_d = \int_{\phi_d}^{\infty} \exp[-\pi W(\phi)R^2/Q]p(\phi)d\phi \Big/ \int_{-\infty}^{\infty} \exp[-\pi W(\phi)R^2/Q]p(\phi)d\phi \tag{5}$$

The calculations shown in Fig. 2 are for an eruption column and flow with constant temperature 450 °C and with interstitial gas in which air and water vapour are present in equal amounts. Ambient air is 10 °C. Hence ρ_l, ν, and ρ_a are 0.4 kg m^{-3}, 0.8 cm^2 s^{-1} and 1.2 kg m^{-3}, respectively. We assume an average value ρ_p of 1,000 kg m^{-3} and, following Wilson's observations[2], that particle sizes in the source eruption column were (approximately) uniformly distributed in the size range (7ϕ)–(-7ϕ).

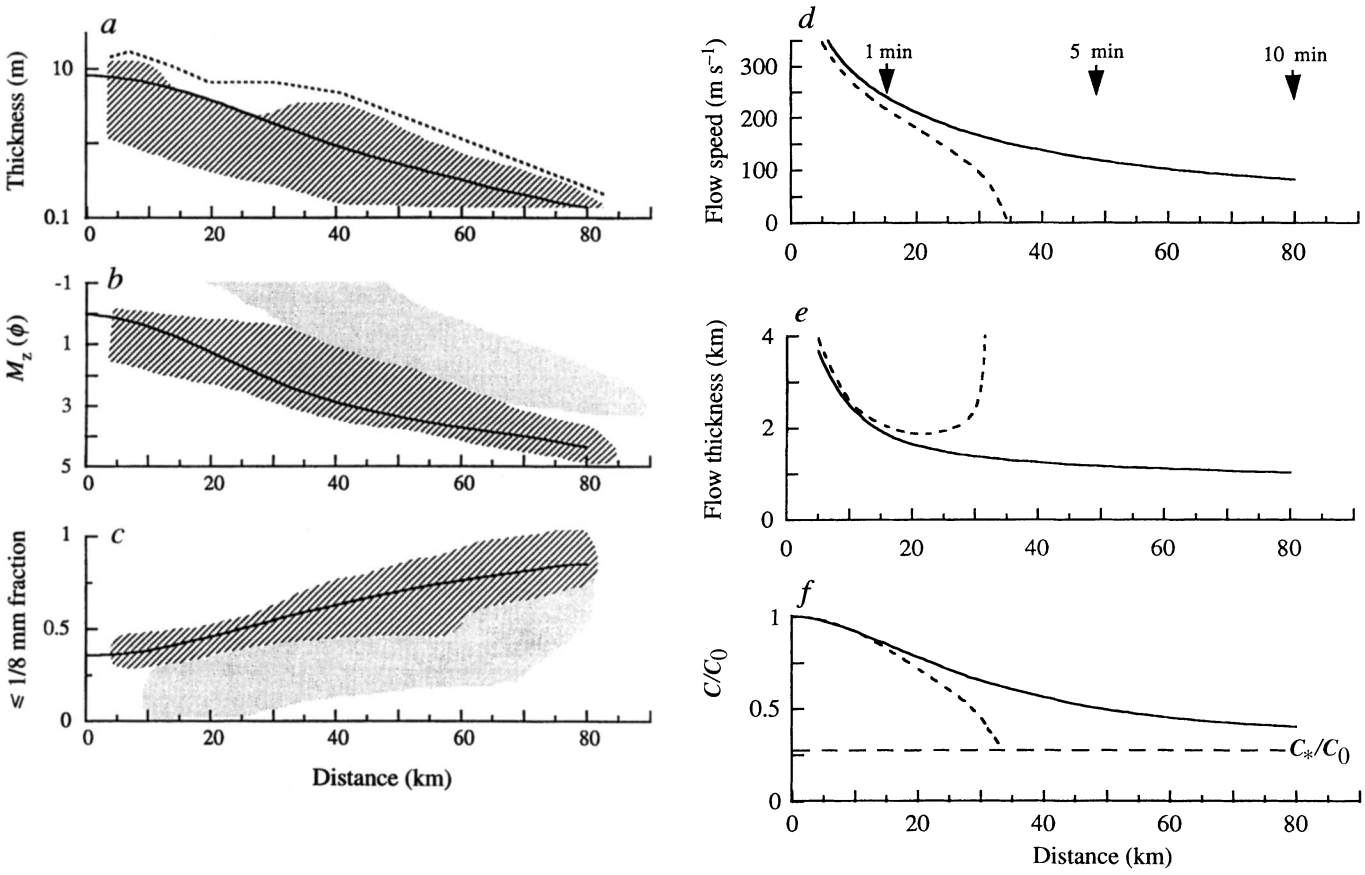

FIG. 2 Characteristics of the Taupo ignimbrite and the parent flow. Radial trends in deposit characteristics as follows. *a*, Deposit thickness. *b*, Graphic mean grain size M_z in units of ϕ, where $\phi = -\log_2$ (diameter in mm) (see ref. 2). *c*, Fraction of material smaller than or equal to 1/8 mm (3ϕ). Characteristics of a reconstructed parent flow for which the temperature and particle concentration in the eruption column were respectively 450 °C and 3 kg m^{-3}. *d*, Flow speed. *e*, Flow thickness. *f*, Concentration of solids relative to concentration at the vent. The shaded regions in *a*–*c* indicate the range of existing observations[2] for the veneer deposit found throughout the Taupo region. The grain-size data do not include the pumice concentration zones and so are biased to finer (larger ϕ) sizes. The dashed line in *a* shows the observed total thickness if maximal estimates for the thickness of layer 1 are included. The lightly stippled regions in *b* and *c* indicate lateral sorting trends in the relatively coarse layer 1 deposits. The solid lines in *a*–*f* show model calculations for the polydisperse suspension observed within the bulk deposit. The short-dashed lines in *d*–*f* represent model calculations for a suspension characterised by a single fall speed of particles (4 m s^{-1}) corresponding to that for the median grain size of 1 mm. The horizontal dashed line in *f* indicates the relative concentration $C_*/C_0 = 0.27$ (~1 kg of solids per m^3) at which the model flow would have become neutrally buoyant.

large-scale, downstream variations in a turbulent flow and its deposit, rather than the depositional system that results in features in the deposit observed on outcrop scale[22,23].

Inputs to the model include material properties for solid and fluid phases. The results are relatively insensitive to exact values of these properties if they are within environmentally imposed constraints. Here we assume that the average density of individual particles is 1,000 kg m^{-3}, that the temperature of the eruption column and flow was 450 °C and that air and water in the interstitial gas were present in equal amounts. Beyond the general assumption of a dilute state, we do not assume *a priori* a specific value of initial solids concentration in the parent flow. Rather, we calculate the concentration of solids using our model and the constraints imposed upon it by the deposit. There are no freely adjustable parameters in the model.

With the incorporation of the known thickness of accumulation near the vent and the bulk grain-size characteristics of the entire deposit (ref. 2), our model predicts radial trends in the thickness and sorting of grain sizes which are in good agreement with Wilson's observations for the veneer deposit (Fig. 2*a*–*c*). An important exception is that the sediments in layer 1 are generally coarser than the overlying veneer deposit as a result, perhaps, of the intense processes of sorting and elutriation associated with the mixing of ambient air into the flow front. The veneer deposit, in combination with the granulometrically similar ponded facies, nevertheless comprises a significant fraction of the overall volume of the ignimbrite and reflects deposition from the main body of the parent flow. Accordingly, it is this depositional unit which is most indicative of the regional transport system in the parent flow. Our model describes the process of particle sorting in the downstream direction based on differences in the settling speeds of individual grains. The good agreement shown in Fig. 2 between predicted and observed measures of deposit thickness (representing a weighted accumulation of all grain sizes), mean grain size and the distribution of fines implies that all grain sizes in the ignimbrite are in approximate aerodynamic equilibrium (as are the largest pumices and lithic fragments discussed above).

Using our model, we infer from the deposit that the total volumetric flux in the turbulent parent flow was of the order of 40 km^3 s^{-1}. No additional parameters are required for the model predictions for the deposit characteristics shown in Fig. 2*a*–*c*. This simplicity constitutes a potentially powerful result of our analysis. We also note, however, that conservation of mass during a finite period of constant flux constrains the concentration of solids in the collapsing eruption column to have been about 3 kg m^{-3}. This degree of expansion means that the associated ash flow was of the order of 1 km thick and advanced at a speed initially in excess of 250 m s^{-1}. It reached the 80-km extent of the known deposit in no

more than about 15 minutes, by which time the eruption apparently ceased and the ash flow dissipated. Our reconstruction of the deposit-forming flow is presented in Fig. 2*d*–*f*. These show, among other things, that the extended runout of the flow beyond about 40 km was due to the presence of fine particles in the parent suspension.

The total flux and near-vent solids concentration inferred for the Taupo event represent values which resulted form the collapse of the eruption column combined with continued discharge of new material at the vent. These values accordingly impose an upper limit on the rate of magma eruption of 5×10^7 m^3 s^{-1}. Given our assumptions regarding temperature and relative vapour content, this suggests that ejecta in the eruption column were at approximately 700 °C and that the fraction of water vapour was about 5% by weight. This result is consistent with independent estimates of water content in the eruption column[24]. Such conditions correspond to a scenario in which material erupted at vertical speeds in excess of 300 m s^{-1} from a vent with a radius of almost 1 km into a collapsing, fountain-like column[25]. The extensive dilution of vented material in the column, and thus its mobility in the resulting turbulent pyroclastic current, reflect the extreme explosivity of the eruption. Preliminary results of detailed calculations indicate that subtle changes in the inferred initial properties of the parent flow do not alter the basic picture presented here.

We are confident that additional details of the Taupo deposit can be reconciled with more sophisticated models for turbulent-flow emplacement. Some near-vent features of the ignimbrite, for instance, may be the result of inhomogeneities in particle concentration in the parent eruption column[26]. Abrupt changes in fines and lithic contents in the ponded deposits at distances of 50–60 km from the vent, on the other hand, may reflect changes in the degree of stratification of the transporting flow[15,22] or interaction of the flow with regional topography which, on average at these distances, comprises ridge-like obstacles that are 500–1,000 m above vent level. These details are qualitatively consistent with our approach but are not explicitly accommodated.

The ease with which our quantitative model can predict regional patterns in deposit characteristics at Taupo argues strongly for the reconsideration of other ignimbrites with similar geometry and sorting trends previously interpreted solely in terms of the prevailing model of emplacement by a highly concentrated flow. Broad consistency of field data with a turbulent-flow model alone does not, of course, exclude other mechanisms of emplacement. In our view, an important challenge is to determine additional deposit properties which can be used to differentiate emplacement mechanisms and relate these to eruption history and associated volcanic hazards. A potentially powerful tool in this regard is the measurement of anisotropy of magnetic susceptibility[27] which reveals the fabric of iron-bearing, elongate grains in a deposit which, in turn, is related to the mechanism of emplacement. Given the current developments in both theory and observation, we suggest that the term 'low-aspect-ratio ignimbrite' be applied only to the physical characteristics of a deposit, and be stripped of connotations regarding the mechanism of emplacement. □

Received 13 September 1995; accepted 22 April 1996.

1. Sparks, R. S. J., Self, S. & Walker, G. P. L. *Geology* **1,** 115–118 (1973).
2. Wilson, C. J. N. *Phil. Trans. R. Soc. Lond.* A **314,** 229–310 (1985).
3. Fisher, R. V. *Am. J. Sci.* **264,** 287–298 (1966).
4. Wilson, C. J. N. & Walker, G. P. L. *Phil. Trans. R. Soc. Lond.* A **314,** 199–228 (1985).
5. Walker, G. P. L., Heming, R. F. & Wilson, C. J. N. *Nature* **283,** 286–287 (1980).
6. Valetine, G. A. & Fisher, R. V. *Science* **259,** 1130–1131 (1993).
7. Simpson, J. E. *Acta mechanica* **63,** 245–253 (1986).
8. Hallworth, M. A., Phillips, J. C., Huppert, H. E. & Sparks, R. S. J. *Nature* **362,** 829–831 (1993).
9. Hallworth, M. A., Huppert, H. E., Phillips, J. C. & Sparks, R. S. J. *J. Fluid Mech.* **308,** 289–311 (1996).
10. Branney, M. J. & Kokelaar, P. *Bull. volcan.* **54,** 504–520 (1992).
11. Druitt, T. H. *J. Volcan. geotherm. Res.* **65,** 27–39 (1995).
12. Wilson, C. J. N. *Bull. volcan.* **50,** 350–351 (1988).
13. Batchelor, G. K. *An Introduction to Fluid Mechanics* (Cambridge Univ. Press, 1983).
14. Clift, R., Grace, J. R. & Weber, M. E. *Bubbles, Drops, and Particles* (Academic, London, 1978).
15. Valentine, G. A. *Bull. volcan.* **50,** 352–355 (1988).
16. Voight, B. *Rockslides and Avalanches, Dev. Geotech. Eng.* Vol. 14A (Elsevier, Amsterdam, 1978).
17. Pickering, K. T., Hiscott, R. N. & Hein, F. J. *Deep Marine Facies* (Unwin Hyman, London, 1989).
18. Kneller, B. C. & Branney, M. J. *Sedimentology* **42,** 607–616 (1995).
19. Dade, W. B. & Huppert, H. E. *J. geophys. Res.* **100,** 18597–18609 (1995).
20. Hopfinger, E. J. *A. Rev. Fluid Mech.* **15,** 47–76 (1983).
21. Dade, W. B. & Huppert, H. E. *Geology* **22,** 645–648 (1994).
22. Valentine, G. A. *Bull. volcan.* **49,** 616–630 (1987).
23. Fisher, R. V. *Geol. Soc. Am. Bull.* **102,** 1038–1054 (1990).
24. Dunbar, N. W. & Kyle, P. R. *J. Volcan. geotherm. Res.* **49,** 127–145 (1992).
25. Sparks, R. S. J., Wilson, L. & Hulme, G. *J. geophys. Res.* **83,** 1727–1739 (1978).
26. Anilkumar, A. V., Sparks, R. S. J. & Sturtevant, B. *J. Volcan. geotherm. Res.* **56,** 145–160 (1993).
27. Fisher, R. V. *J. Volcan. geotherm. Res.* **56,** 205–220 (1993).
28. Bonnecaze, R. T., Huppert, H. E. & Lister, J. R. *J. Fluid Mech.* **294,** 93–121 (1995).

ACKNOWLEDGEMENTS. R. Cas, T. Druitt, D. Pyle, S. Sparks, G. Valentine, C. Wilson and A. Woods provided constructive and challenging discussions of pyroclastic flows and ignimbrites, although not all agree with the views presented here.

Eusociality in a coral-reef shrimp

J. Emmett Duffy

School of Marine Science and Virginia Institute of Marine Science, The College of William and Mary, Gloucester Point, Virginia 23062, USA

The apex of animal social organization is eusociality, which has three characteristics: overlapping generations, reproductive division of labour, and cooperative care of young[1,2]. So far, eusociality has been recognized only among social insects and the African mole-rats[3–5]. Here I report the first case of eusociality in a marine animal. The sponge-dwelling shrimp *Synalpheus regalis* lives in colonies that may have >300 individuals, but that contain only one reproductive female. Direct-developing juveniles remain in the natal sponge, and allozyme data suggest that most colony members are full sibs. In laboratory experiments, larger colony members, most of whom apparently never breed, defended the colony against heterospecific intruders. Ecological similarities among mole-rats, termites and these sponge-dwelling shrimp, all of which are diploid animals, strengthen arguments that eusociality is favoured by gradual metamorphosis, parental care, and occupation of protected, expansible niches[6].

The mobile cryptofauna of coral reefs is frequently dominated by snapping shrimps (*Synalpheus*)[7–9], many of which live within the internal canals of sponges. *S. regalis* is an abundant cryptofaunal species at Carrie Bow Cay, Belize, and inhibits the sponges *Xestospongia* cf. *subtriangularis* and *Hyattella intestinalis*[9,10]. Each of over 30 dissected sponges contained a colony of *S. regalis* consisting of 3–313 individuals ($\bar{x} = 149$, from 17 complete colonies examined). As tropical *Synalpheus* species apparently breed continuously (J.E.D., personal observation), reproductive females are easily identified by ripe ovaries or brooded eggs, yet each colony invariably contained only a single reproductive female. The remaining juveniles and mature males are difficult to distinguish morphologically, probably reflecting a socially mediated sex-determination system, as is known in another alpheid[11]. By having just one female, these colonies clearly meet the first criterion of reproductive division of labour.

Eusociality also requires that generations overlap[2], bringing individuals into contact with close kin such that altruistic behaviours can be favoured by kin selection[12]. Three lines of evidence indicate that *S. regalis* colonies consist primarily of sibling offspring of the lone female (the 'queen'). First, *S. regalis* eggs hatch into crawling juveniles; successive cohorts of small juveniles are clearly recognizable in many colonies, suggesting that they nor-